In-Situ Raman Spectroscopy of α- and γ-FeOOH during Cathodic Load

K. Hedenstedt,[a,b] J. Bäckström,[a,c,z] and E. Ahlberg[a]

[a]*Department of Chemistry and Molecular Biology, University of Gothenburg, SE-41296 Gothenburg, Sweden*
[b]*AkzoNobel Pulp and Performance Chemicals, SE-44580 Bohus, Sweden*
[c]*Department of Natural Sciences, Mid Sweden University, SE-85170 Sundsvall, Sweden*

Water reduction on corroded iron surfaces is technologically and fundamentally important. Here, the technological interest originates from the chlorate process where water reduction is the main cathodic process. Fundamentally, water reduction on oxide surfaces raises questions on the stability of the oxide and the nature of electrocatalytic surface sites. Two iron oxyhydroxides, α- and γ-FeOOH, were electrodeposited on titanium substrate and their reduction processes were followed in detail with in-situ Raman spectroscopy, using low incident laser power to avoid sample damaging. Polarization to negative potentials show two reduction peaks for γ-FeOOH and one peak for α-FeOOH prior to hydrogen evolution. The characteristic Raman peaks gradually disappear as the potential is made more negative but no new peaks can be observed. δ-FeOOH was detected as an intermediate phase upon oxidation of the reduced surface layer. This indicates that $Fe(OH)_2$ is formed during cathodic polarization and initially re-oxidized to the isostructural δ-FeOOH. Characteristic Raman signals of the original phases appear upon further oxidation in air.
 [DOI: 10.1149/2.0731709jes]

Manuscript submitted May 1, 2017; revised manuscript received June 19, 2017. Published July 8, 2017.

Industrial electrochemical processes are extraordinarily energy demanding. For example, about 18 TWh of electricity is used every year world-wide to produce sodium chlorate ($NaClO_3$) by electrolysis.[1] At the anode Cl^- is oxidized to Cl_2 which undergo subsequent reactions in the liquid phase to form chlorate. The anode material is commonly a dimensionally stable anode (DSA) consisting of titanium metal with a coating of $Ti_{1-x}Ru_xO_2$. The cathode is often made of mild steel and the main cathode reaction is hydrogen evolution. Side reactions occur both on the anode and the cathode side, lowering the current efficiency of the process.

The main corrosion products found on mild steel electrodes operated under slightly different operating conditions are goethite (α-FeOOH) or lepidocrocite (γ-FeOOH). These products show different current efficiencies in the chlorate process and in two recent papers kinetic parameters for hypochlorite and water reduction were obtained.[2,3] Reduction of hypochlorite is the main side reaction in the chlorate process and is mainly inhibited by adding chromate to the electrolyte. No differences in the rate of hypochlorite reduction between the two oxyhydroxide phases were obtained.[3] The rate of water reduction is initially lower on α-FeOOH and γ-FeOOH compared with a mild steel electrode due to prior reduction of the oxyhydroxide phases as such. Once reduced at the oxide electrolyte interface, the rate of hydrogen evolution is the same.[2] This suggests that the active site for hydrogen evolution is the same on all three materials, i.e. a reduced site.

The complex electrochemical behavior of iron in aqueous solution has been studied in detail in the corrosion community[4–11] and is well described. Reduction of γ-FeOOH on other substrates has been studied previously and there is a general understanding that $Fe(OH)_2$ is formed. Depending on pH and composition of the electrolyte also magnetite can be formed, preferentially by a dissolution precipitation reaction.[12–15] In-situ techniques such as Mößbauer[9] and Raman[5,7,11] spectroscopy as well as X-ray diffraction (XRD) and X-ray absorption spectroscopy (XAS)[4] have been used to track the state of the surface during electrochemical polarization. In most cases neutral to slightly alkaline or strongly alkaline solutions were used, where the reduction of iron oxides and hydroxides yield soluble Fe(II) species.

In the present study in situ Raman spectroscopy was employed to study the reduction and re-oxidation of α-FeOOH and γ-FeOOH deposited on titanium substrates. The pH was set to 11 in order to mimic the operational conditions at hydrogen evolution and with the aim to detect any changes in the composition of the surface layer upon polarization.

Experimental

Samples.—The two phases of FeOOH were prepared both as bulk powder and as electrode coatings on Ti-metal substrates. The phase purity was checked using XRD.

Electrodes.—Martinez et al.[16] have shown a simple electrodeposition synthesis route of α- and γ-FeOOH with only Mohr's salt and potassium acetate. This method was used as basis for the sample preparation. Pieces of 2 cm × 1 cm were cut out from titanium grade 1 (i.e. commercially pure) sheets and welded to titanium rods of diameter 2 mm. The rods were covered with Teflon tape to maintain a controlled surface area. The surface was polished with 1000 grit SiC paper (Struers) and rinsed with 18 MΩcm Milli-Q water. Electrolyte was prepared as described with 0.01 M Mohrs salt (Sigma Aaldrich ReagentPlus grade) and 0.04 M potassium acetate (Sigma Aaldrich ReagentPlus grade). It was kept under nitrogen purge at 90°C. The titanium electrode was pickled with 5% hydrofluoric acid (BASF electronic VLSI grade) for 10 seconds and rinsed with Milli-Q water just seconds before deposition. The deposition took place at −150 mV vs Ag/AgCl (3 M KCl) for α-FeOOH and +1000 mV for γ-FeOOH. A total charge of 2 $C \cdot cm^{-2}$ was passed during deposition. Rotating disk electrodes were prepared on 1 cm^2 titanium disks for linear-sweep voltammetry tests using the same deposition procedure.

Bulk samples.—Bulk (powder) samples were also produced to verify the Raman peaks for the different iron oxyhydroxides. The preparation of α-FeOOH and γ-FeOOH followed the recipes according to Schwertmann and Cornell.[17] The choice of starting material was $FeCl_2 \cdot 4H_2O$ (Sigma Aaldrich ReagentPlus grade) since it worked for the synthesis of both phases. NaOH and $NaHCO_3$ used were from Sigma Aaldrich (ReagentPlus grade). After synthesis the dispersions were filtered and dried at 45°C over night.

Sample characterization.—XRD was performed on the electrodeposited electrode samples with a Siemens D5000 diffractometer with a Cu K_α source (wavelength 1.54 Å). The bulk (powder) samples have been analyzed and verified with XRD previously[2] and found to be of good quality.

Electrochemical measurements.—For electrochemical measurements, a fine platinum mesh as counter electrode and Ag/AgCl

[z]E-mail: joakim.backstrom@miun.se

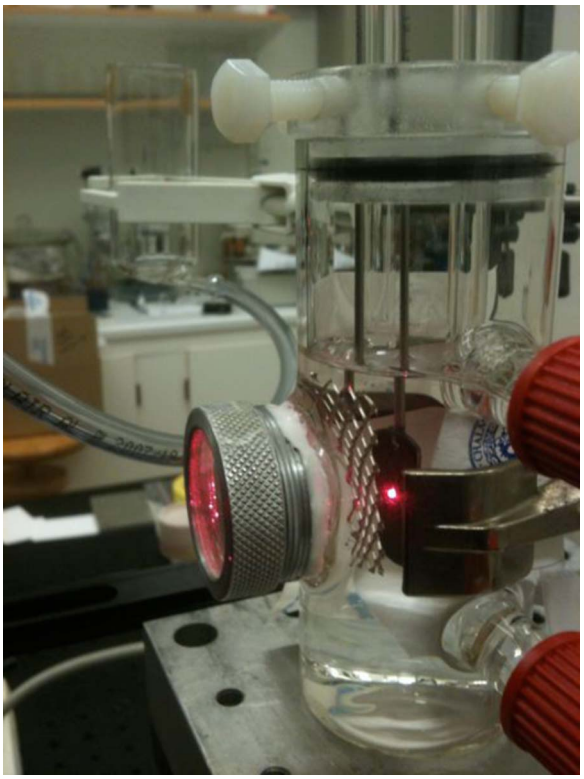

Figure 1. Photograph of the in situ Raman cell used in the study.

reference electrode with 3 M KCl were used. The electrolyte was 0.2 M Na_2SO_4(aq) (Sigma Aaldrich ReagentPlus) with pH 11 set with NaOH (Sigma Aaldrich ReagentPlus). The electrolyte was purged with nitrogen gas for at least 30 minutes prior to measurements.

A Gamry reference 600 potentionstat was used for steady-state measurements. Potential steps of 50 mV were made from −500 to −1250 mV vs Ag/AgCl on flag electrodes while Raman measurements were performed on each step. Steady state current was obtained 15 minutes after setting the potential.

A Solartron 1287 potentiostat was used for analog sweeps. The analog sweeps were made using rotating-disk electrodes with rotation speed 3000 min^{-1} and sweep rate 0.1 mVs^{-1}.

In-situ Raman spectroscopy.—The measurements were made using a Dilor XY800 spectrometer working in short (focal length 300 mm) single-grating mode using holographic notch filters for rejection of photons with the excitation-line wavelength. The excitation source was a mixed-gas Ar^+/Kr^+ laser capable of producing a large number of lines in the visible region. The experiment was carried out in a back-scattering geometry with the sample situated in an electrochemical glass cell with quartz-glass window. The cell is pictured in Figure 1. The incoming light was focused on the working electrode inside the cell using a positive lens with 8 cm focal length. The scattered light was collected through the same lens.

For all Raman spectroscopy measurements, the laser power incident on the sample was kept very low (about 1–2 mW) to avoid any laser-induced damage to the material. Other groups have previously reported that these materials are very sensitive to damage due to intense light.[12] We performed experiments on the bulk powder samples with varying laser powers, and concluded that 2 mW was within good margin on the safe side for powder samples in air. It is likely that electrode coatings on metal substrates immersed in liquid electrolyte could withstand higher powers without damage, due to better heat dissipation. However, low laser power was still used to avoid risks of damaging the samples.

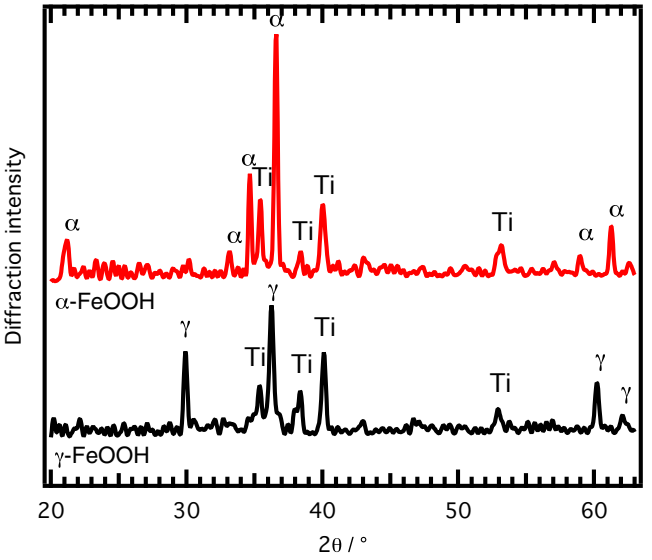

Figure 2. X-ray diffraction patterns, using Cu K_α radiation, of electrode samples. The position of peaks from α- and γ-FeOOH as well as titanium metal, as known from databases are indicated. The curves are offset vertically for clarity.

Incoming light was polarized in the direction where the spectrometer shows highest sensitivity (horizontal for 514 nm, vertical for 647 nm). No polarization filter was used to filter the analyzed, scattered light. A liquid-nitrogen cooled charge-coupled device was used as photodetector. The Raman spectra in this paper are displayed without further treatments or data corrections, except for removal of spikes originating from cosmic radiation impinging the detector.

A Luggin capillary with the opening about 1 mm in front of the working electrode was used to connect the Ag/AgCl reference electrode via an electrolyte bridge. The electrolyte was deaerated using N_2 purging. A mesh of platinum was used as counter electrode. All experiments were carried out at room temperature.

Results and Discussion

Sample characterization.—The prepared electrode samples were measured using XRD. The results were compared to known data from the two iron oxyhydroxide phases of interest, goethite (α-FeOOH) and lepidocrocite (γ-FeOOH) to assure phase purity. Figure 2 displays the XRD patterns from electrode samples of both FeOOH phases. All discernible reflections could be attributed to either α-FeOOH or γ-FeOOH, respectively, or to the titanium-metal substrate.

Raman spectra were first measured from powder samples of goethite (α-FeOOH) and lepidochrocite (γ-FeOOH) using several different laser wavelengths. It was found that the signal strength was maximum using the red 647 nm line of the Ar^+/Kr^+ laser, among the tested lines. Comparison between excitation with 514 nm and 647 nm is shown in Figure 3. One can clearly see that the strength of the signal when using the red excitation line is higher than using the green line. This holds for both FeOOH phases and agrees to some extent with the findings of Nieuwoudt et al.,[18] where a clear resonance enhancement was found toward the red part of the spectrum for several iron oxides and oxyhydroxides (though they found the maximum around 633 nm).

The wavelength giving the highest signal, 647 nm (photon energy 1.92 eV), relates to the transition between the ground state $^6A_1$ to the excited ligand field state $^4T_2$ (^4G) and gives rise to resonance and higher intensities of the peaks. The relevant transition at 514 nm wavelength (photon energy 2.41 eV) relates to the double exciton process, where two magnetically coupled Fe(III) ions in the structure are excited at the same time.[19]

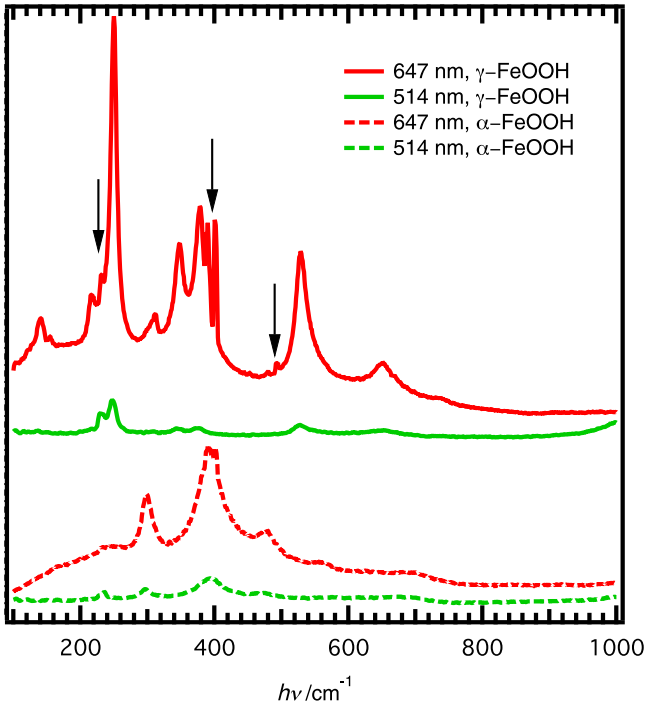

Figure 3. Ex situ Raman spectra of α- and γ-FeOOH powder samples using red (647 nm) and green (514 nm) excitation laser lines. The spectra are offset vertically for clarity. In the measurement of γ-FeOOH using red laser line, some spurious spectral lines (confirmed to originate from illumination of the hallway outside the laboratory) appeared, indicated by arrows.

The conclusion from our investigation of Raman signal strength as function of excitation wavelength was that the red line at 647 nm gave a good signal and was thus used as standard choice for the remainder of the study. Figure 4 display the ex situ spectra, using 647 nm laser excitation line, of both the α-FeOOH powder sample and the γ-FeOOH powder sample. Included in the graphs are the known positions of Raman lines from several articles found in the literature of the two materials. The spectra of our powder samples correspond very well to previously reported data, confirming that the α- and γ-phases of FeOOH are easily distinguished from each other using Raman spectroscopy. From the XRD data and the quality of the Raman spectra we conclude that the samples are of high level of phase purity.

In situ electrochemical Raman spectroscopy.—When the electrode sample is located inside an electrolyte-filled cell, the Raman signal from the electrode material will inevitably be superimposed on the spectrum of the electrolyte. Figure 5 shows three Raman spectra measured inside the experiment cell, more precisely spectra of the bare electrolyte (0.2 M Na_2SO_4(aq), adjusted to pH 11 using NaOH), an α-FeOOH electrode in a dry cell, and an α-FeOOH electrode in an electrolyte-filled cell (not connected to any voltage source). It can be noted that the bare-electrode spectrum is very similar to the powder-sample spectrum in Figure 4. In addition, since this is a broader scan, there are features visible around 1200–1500 cm^{-1}, that also belong to α-FeOOH.[21]

The spectrum of the sample inside the electrolyte is clearly a straightforward combination of the individual sample and electrolyte spectra. It can also be noted that (i) the strong diffuse scattering from the aqueous electrolyte at low energies prevents any useful analysis of FeOOH peaks below about 300 cm^{-1} and (ii) the strong symmetric stretching vibration mode of SO_4^{2-} at 981 cm^{-1} can usefully serve as an internal signal-strength standard for the in situ Raman measurements.

Figure 6 shows a series of Raman spectra measured with the α-FeOOH cathode held at different potentials. The spectra were recorded consecutively, starting with an open-circuit potential (OCP) measurement, ending with a cathode potential of −1050 mV vs Ag/AgCl. Also shown in the figure are the steady-state current densities measured after 1000 seconds of stabilization at each potential. It can be seen that the Raman lines attributable to α-FeOOH (most notably at 290 cm^{-1}, 390 cm^{-1} and 660 cm^{-1}, compare Fig. 4) slowly decrease as the sweep proceeds toward more negative potentials, while the sulfate peak at 981 cm^{-1} from the electrolyte stays at the same intensity. This is a clear indication that the material is affected by the cathodic load.

Note that there is no gas evolution in the cell, i.e. an explanation of the decreased Raman-peak intensities based on disturbance of the optical path by bubbles can be ruled out. Another sign that the decrease in Raman signal is real, is that the sulfate peak at 981 cm^{-1} is unaffected by the electrochemical polarization. It can further be seen that the current flow is very low at potentials above −0.90 V vs Ag/AgCl, but grows thereafter to −0.22 mA/cm^2.

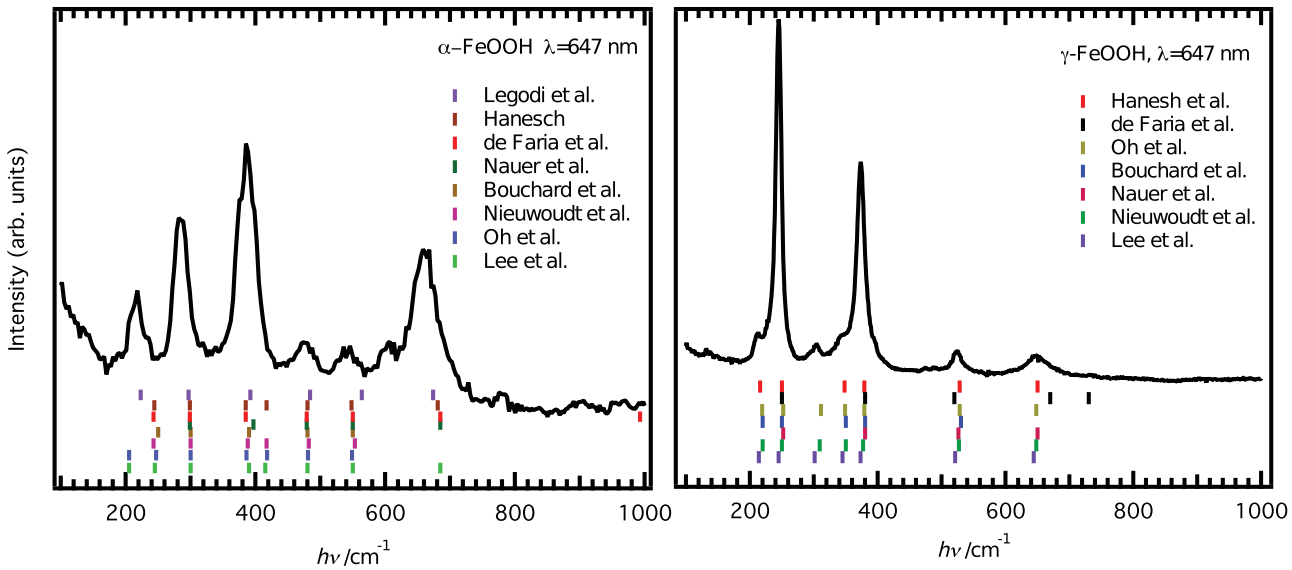

Figure 4. Ex situ Raman spectra of α- and γ-FeOOH powder samples measured using 647 nm excitation wavelength. Raman-mode observed by other authors are indicated.[12,18,20–25]

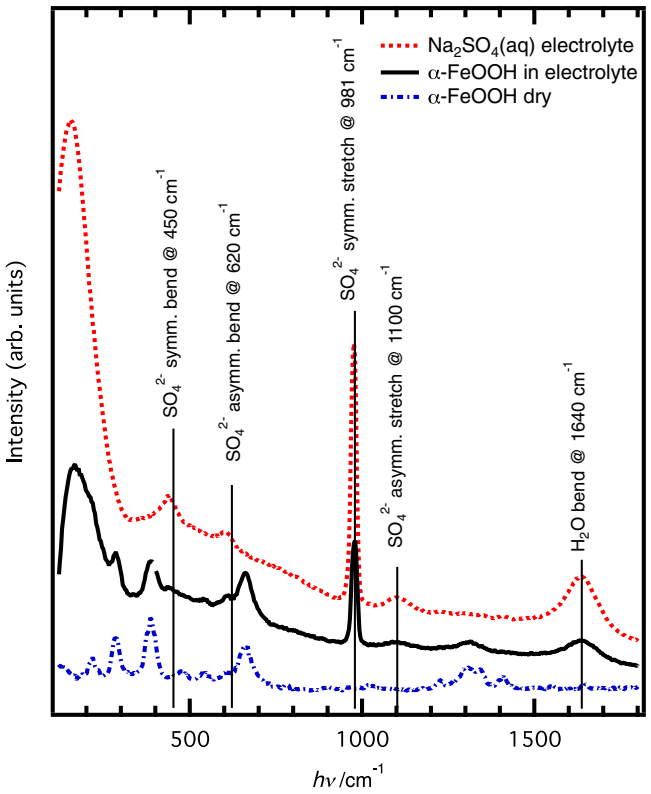

Figure 5. Raman spectra from α-FeOOH sample inside the cell without electrolyte, spectra from the 0.2 M Na_2SO_4 electrolyte (set to pH 11 using NaOH) itself, and the sample measured in the electrolyte-filled cell. The known modes from water and sulfate ions are labeled.[26–28] The 647 nm laser line was used as excitation source. The three spectra have been offset vertically and rescaled to facilitate comparison.

Figure 7 shows the corresponding data for γ-FeOOH. It is evident that the Raman-line intensities decrease more rapidly than for the α-phase. It is also evident that the potential dependence of the current density is quite different from what is observed for the α-phase. There is a reduction peak at a potential of −0.9 V vs Ag/AgCl that has no counterpart in α-FeOOH. The currents are overall larger.

To investigate the differences in electrochemical behavior of the two FeOOH phases, very slow potentiodynamic sweeps were performed. Polarization to negative potentials shows two reduction peaks for γ-FeOOH and one peak for α-FeOOH prior to hydrogen evolution, Figure 8. It should be noted, that these sweeps were repeated a number of times using different, freshly prepared, electrodes, with very similar results. In other words, both the double-peak structure of the curve for γ-FeOOH and the peculiar shape of the reduction peak seen in α-FeOOH are real.

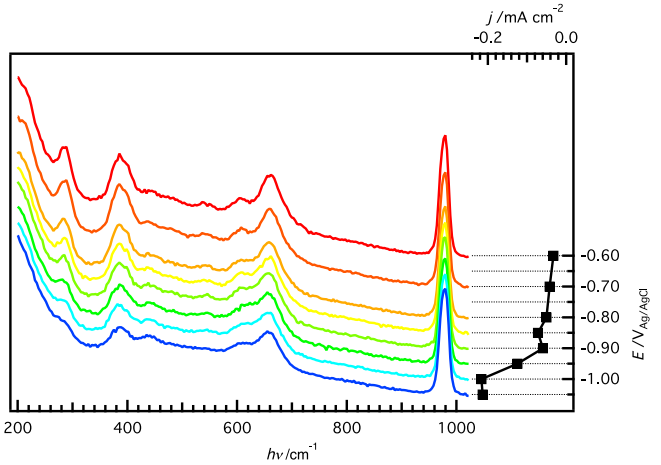

Figure 6. Evolution of Raman spectra with increasing cathodic load for α-FeOOH using laser wavelength of 647 nm, together with steady-state currents for each potential. Each Raman spectrum is offset vertically to connect to the potential at which it was measured, as displayed on the right-hand scale.

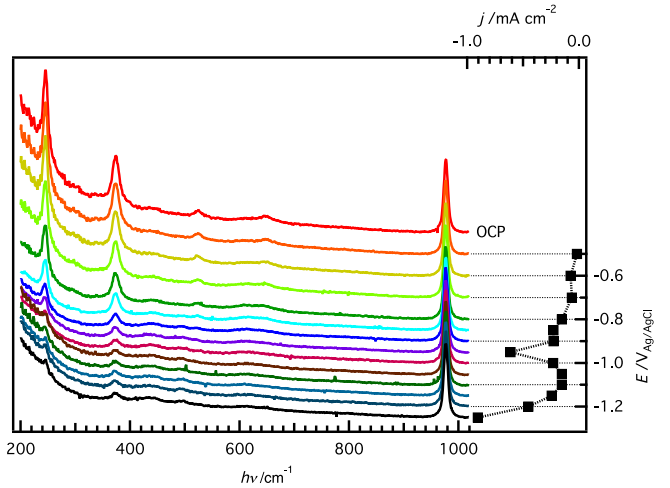

Figure 7. Evolution of Raman spectra with increasing cathodic load for γ-FeOOH using laser wavelength of 647 nm, together with steady-state currents for each potential. Each Raman spectrum is offset vertically to connect to the potential at which it was measured, as displayed on the right-hand scale.

The voltammetric response of precipitated iron hydroxides on inert substrate as well as corrosion products on iron in alkaline solution shows several oxidation and reduction peaks related to oxidation of iron metal to $Fe(OH)_2$, $Fe(OH)_2$ to FeOOH and reduction of FeOOH to $Fe(OH)_2$ and Fe_3O_4 to $Fe(OH)_2$.[5] The number of peaks and the position on the potential scale depends on the nature and thickness of the layer, pH and composition of the electrolyte. At the pH value used in the present paper $Fe(OH)_2$ has its lowest solubility with micromolar concentrations of the neutral hydrolysis complex $Fe(OH)_2$ (aq). Under these circumstances the reduction of the oxyhydroxides probably proceeds through a solid-state mechanism.[2] The charge associated with

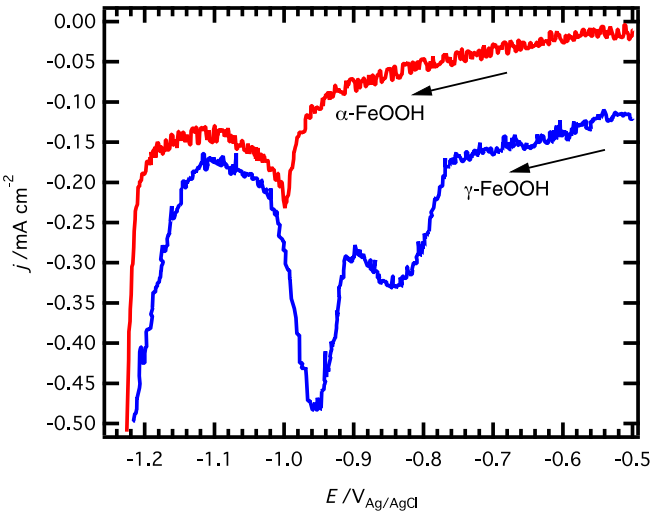

Figure 8. Slow potentiodynamic sweeps on both α- and γ-FeOOH, clearly indicating the presence of a reduction peak at about −0.85 V vs. Ag/AgCl, unique for the γ-phase. Sweep rate was 0.1 $mV \cdot s^{-1}$. Sweep direction indicated by arrows.

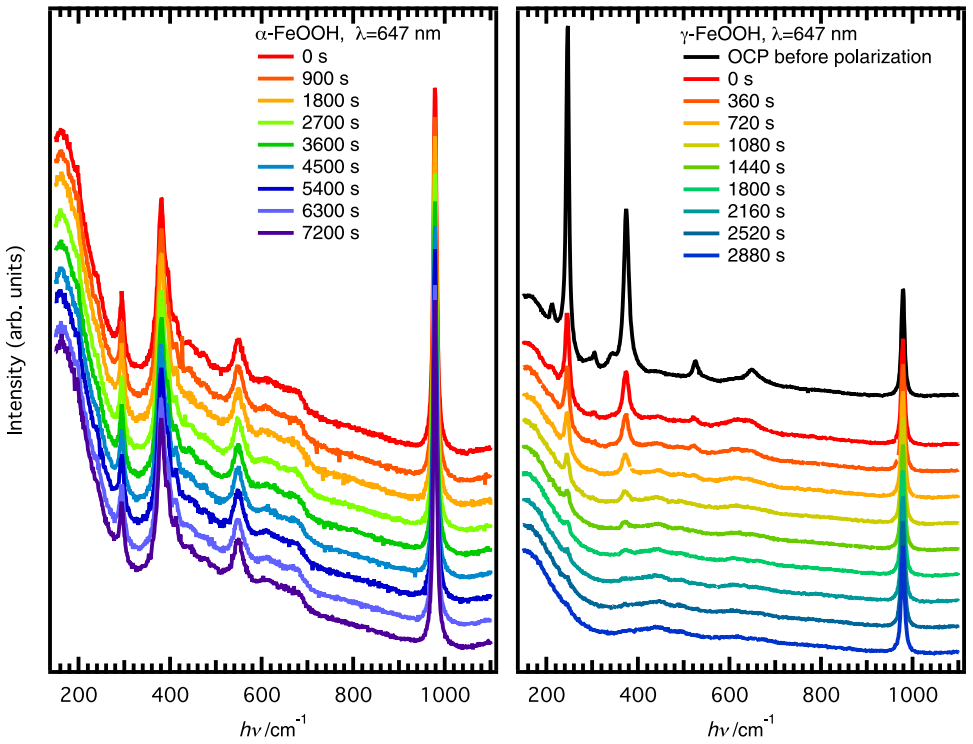

Figure 9. Evolution of Raman spectra with time during cathodic load of −950 mV vs Ag/AgCl for α-FeOOH and γ-FeOOH using laser wavelength of 647 nm, as indicated. The labeled time points correspond to the time where the accumulation of Raman data commenced, with zero being start of polarization. In the right panel, the spectrum from the same sample before start of electrolysis is included for comparison.

the reduction differ between the two phases. The charge applied in the deposition of the layers were 2 C while the charge associated with the reduction amounts to 3.5% for α-FeOOH and 17.3% for γ-FeOOH, thus only the uppermost layer is reduced during the time of the measurements. The existence of two peaks for γ-FeOOH and one peak for α-FeOOH only appear at the low sweep rate used in the present work. At higher sweep rates, one broad peak is observed for the γ-phase and almost a constant cathodic current for the α-phase prior to hydrogen evolution.[2] The large effect of sweep rate as well as the small charge involved indicate that the reduction kinetics are slow, giving further support for a solid-state reaction mechanism, where the availability of water and transport of produced OH^- might be rate limiting.

In Figure 9, the time evolution of Raman spectra during constant cathodic load of −950 mV vs Ag/AgCl is shown for α-FeOOH and γ-FeOOH. The potential is chosen where the γ-phase shows a pronounced reduction peak, but before the reduction peak of α-FeOOH (compare with Figure 8). The α-phase shows a very small weaking of the Raman lines (the intensity of the 380 cm^{-1} mode decreases about 8% from $t = 0$ to $t = 7200$ s), while all Raman peaks of the γ-phase have practically vanished at $t = 2160$ s. Clearly, the solid material itself undergoes a transformation connected to the −950 mV reduction peak.

The current was also measured as a function of time during polarization. A clear difference in the current-time curves were observed, Figure S1 in supplementary information. For α-FeOOH, the current decreases quickly from start and then asymptotically toward zero. The long time necessary is typical for discharging a capacitor with ionic components. For γ-FeOOH, the initial decrease is halted and the current becomes almost constant for 10 minutes before the current decreases again. The different behavior for the two phases is expected since the applied potential is sufficient to reduce the γ-phase but not the α-phase. For γ-FeOOH, the initial decrease is related to the fast reduction of the γ-phase by the potentials step and is limited by the availability of water. This process is overlapping with phase transformation from γ-FeOOH to $Fe(OH)_2$, supporting the solid state mechanism for reduction of γ-FeOOH in moderate alkaline solutions. A phase transition is also observed for the α-phase polarized at −1050 mV vs Ag/AgCl, where reduction takes place. However, the time necessary for the reduction is much shorter.

For γ-FeOOH, the potentiostatic reduction at −950 mV vs Ag/AgCl was followed with in situ Raman spectroscopy also using the green 514 nm laser line. The data are not shown here, but can be found in the supplementary information (Figure S2). That experiment also demonstrates a disappearance of the Raman lines belonging to γ-FeOOH, very similar to what can be seen in the right panel of 9. This demonstrates that the spectral changes upon cathodic polarization are not likely due to shifting of the Raman resonance out of the red part of the optical spectrum.

Odziemkowski et al.[29] showed that $Fe(OH)_2$ has a low Raman signal that was detected only using surface-enhanced Raman scattering by depositing a discontinuous silver film on top of the electrode. Lutz et al.[30] prepared several brucite-type metal dihydroxides and investigated them using neutron diffraction, Raman spectroscopy and FTIR, showing a Raman spectrum of $Fe(OH)_2$ with weak peaks at 260 cm^{-1} and 407 cm^{-1}. They argued, based on phonon-mode analysis and comparison with isostructural compounds, that a previously reported characteristic peak at 545 cm^{-1} cannot belong to $Fe(OH)_2$. The absence of $Fe(OH)_2$-related peaks in the spectra in this study should not be interpreted as absence of $Fe(OH)_2$. Since $Fe(OH)_2$ is known to be a weak Raman scatterer, its Raman signal is expected to be overshadowed by the stronger signal from the iron oxyhydroxides.

Reoxidation of the γ-FeOOH electrodes.—In Figure 10 the Raman spectra during spontaneous re-oxidation of reduced γ-FeOOH are shown. Spectrum (1) shows the spectrum at open circuit prior to reduction and spectrum (2) shows the spectrum at the end of the polarization sweep shown in Figure 7. As the potential gets more negative the characteristic peaks for lepidocrocite diminish but are still visible. The electrode was disconnected, rinsed in water and then measured again, spectrum (3). By contact with air and water the reduced layer

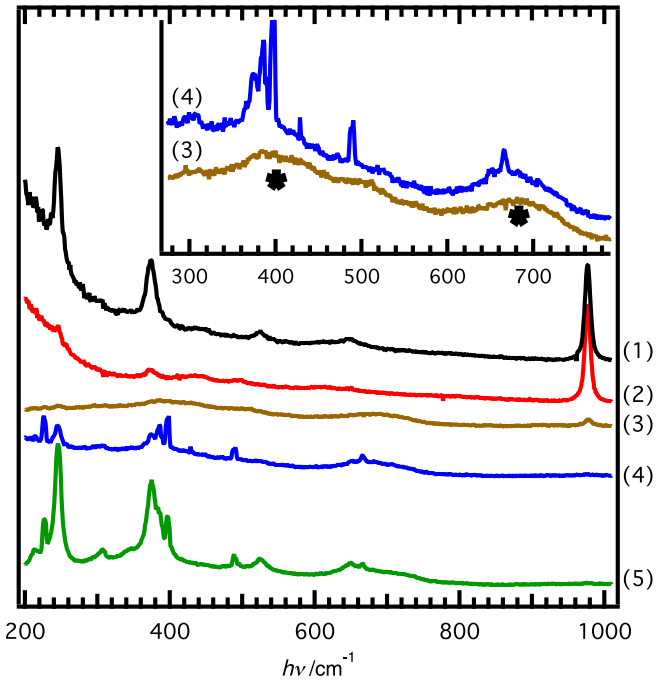

Figure 10. Reoxidation of γ-FeOOH on Ti substrate. First spectrum (1) is measured on the sample before cathodic load under OCP conditions (same as top spectrum in Figure 7). Spectrum (2) shows the sample after it had been subjected to a cathodic polarization series (same as bottom spectrum in Figure 7). Spectrum (3) is measured from the same sample after it had been removed from the electrolyte and rinsed in Milli-Q water. The sample was left in air overnight and measured again, spectrum (4), and finally rinsed again in Milli-Q water and remeasured, spectrum (5). The change in slope in the background toward low Raman shifts is due to higher straylight when measuring in situ. Spectra (4) and (5) displays the same spurious spectral lines as indicated in Figure 3. The inset shows spectra (3) and (4) in a different scale, making the broad bands attributed to δ-FeOOH (marked with asterisks) more clear.

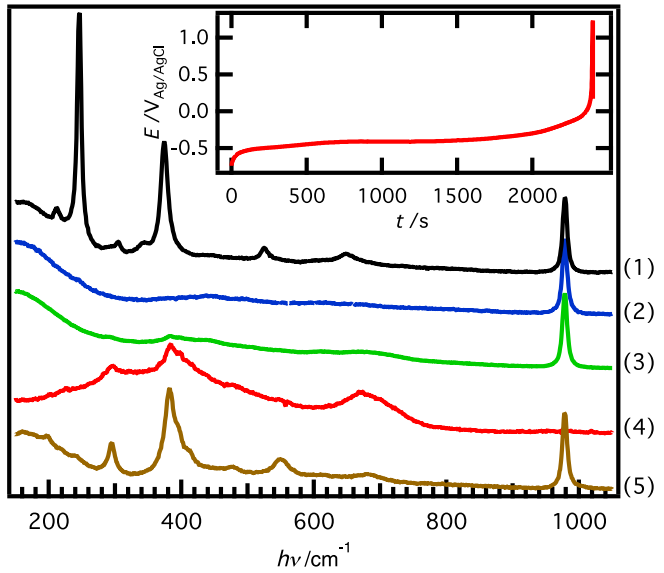

Figure 11. Reoxidation of γ-FeOOH on Ti substrate. First spectrum (1) is measured before cathodic load under OCP conditions. Spectrum (2) shows the sample toward the end to a cathodic polarization series. (Spectra (1) and (2) are identical to top and bottom spectra in the right panel of of Fig. 9) Spectrum (3) is measured from a sample that had been left in the electrolyte overnight after cathodic polarization followed by anodic re-oxidation (see inset). The sample was left in air several hours and measured again, spectrum (4). The bottom spectrum (5) is an in situ spectrum of α-FeOOH without electrochemical polarization for comparison. The spectra are offset vertically for clarity, and rescaled to match the intensity of the sulfate peak at 981 cm^{-1}.

is partly oxidized and two broad bands at about 400 and 700 cm^{-1} are appearing. These bands have been attributed to δ-FeOOH,[12,31] which is isostructural with $Fe(OH)_2$ and can be formed by topotactic conversion of $Fe(OH)_2$.[17,32] δ-FeOOH is a poorly crystalline phase and undergo transformation to lepidocrocite or goethite depending on pH and electrolyte composition.[33] This is also observed in spectrum (4) and (5) measured after exposure to air overnight (4) and subsequently rinsed with water (5). The formation of γ-FeOOH is clearly observed and enhanced by the availability of water in the last step.

Re-oxidation by applying a small constant current density of 0.6 $mA{\cdot}cm^{-2}$, was also performed for a reduced γ-FeOOH layer (the sample reduced by cathodic polarization at −950 mV vs. Ag/AgCl for 2880 s, see Figure 9). The evolution of Raman spectra during the re-oxidation process is displayed in Figure 11, including the simultaneously measured potential-time curve (inset). The potential is fairly constant at about −400 mV vs. Ag/AgCl during the first ∼2000 seconds. Above $t \approx 2300$ s, the potential rises quickly to values where oxygen evolution takes place and the experiment was terminated as the potential reached the preset threshold at $t = 2400$ s. For clarity the Raman spectra for the deposited layer at the open circuit potential is shown in spectrum (1) and the spectrum of the reduced layer in (2). After the galvanostatic measurement the electrode was left in the electrolyte at the open circuit potential overnight. The subsequent Raman spectrum (3) shows peaks related to α-FeOOH together with broad peaks that might be related to the formation of δ-FeOOH. The electrode was removed from the cell and subjected to air for several hours and then re-measured. The peaks related to α-FeOOH are now more pronounced even though the broad peak around 700 cm^{-1} is still observed. Spectrum (5) shows the characteristic peaks for α-FeOOH measured in the electrolyte at the open circuit potential.

The main difference between these two re-oxidation experiments is the accelerated oxidation induced by an applied positive current. This leads to the formation of α-FeOOH while the direct oxidation in air leads to formation of the original material, γ-FeOOH. It is well described in the literature that the formation of one or the other forms of the iron oxyhydroxides can be controlled by pH, rate of oxidation and electrolyte composition.[4,32–34]

Conclusions

Electrochemical in situ Raman spectroscopy has been successfully performed on electrodes of α-FeOOH (goethite) and γ-FeOOH (lepidocrocite) electrodeposited on titanium substrates. We noticed that the Raman signal from both FeOOH phases got weaker under cathodic polarization. We attribute the disappearing of the Raman signal to formation of $Fe(OH)_2$ during reduction.

Reoxidation of mildly reduced γ-FeOOH in air resulted in reappearance of the Raman spectrum characteristic of γ-FeOOH, while reoxidation via anodization of reduced γ-FeOOH resulted in appearance of a Raman spectrum characteristic of α-FeOOH.

δ-FeOOH was detected as an oxidation intermediate between the reduced phase and α- and γ-FeOOH, supporting the formation of $Fe(OH)_2$ under cathodic polarization.

Acknowledgment

Financial support from the Swedish energy agency, 33280-1, the Swedish research council, 621-2010-4035, and AkzoNobel Pulp and Performance Chemicals AB is gratefully acknowledged. The authors thank Permascand for supplying the titanium material and the Condensed Matter Physics group, especially Ezio Zanghellini, at Chalmers University of Technology for granting the Raman spectrometer.

References

1. H. Vogt, J. Balej, J. E. Bennett, P. Wintzer, S. Sheikh, P. Gallone, S. Vasudevan, and K. Pelin, Chlorine oxides and chlorine oxygen acids, Ullman's Encyclopedia for Industrial Chemistry, Wiley-VHC Verlag, Weinheim (2010).
2. K. Hedenstedt, N. Simic, M. Wildlock, and E. Ahlberg, *J. Electroanal. Chem.*, **783**, 1 (2016).
3. K. Hedenstedt, A. S. O. Gomes, M. Busch, and E. Ahlberg, *Electrocatalysis*, **7**, 326 (2016).
4. J. Monnier, S. Réguer, E. Foy, D. Testemale, F. Mirambet, M. Saheb, P. Dillmann, and I. Guillot, *Corros. Sci.*, **78**, 293 (2014).
5. A. Hugot-Le Goff, J. Flis, N. Boucherit, S. Joiret, and J. Wilinski, *J. Electrochem. Soc.*, **137**, 2684 (1990).
6. M. Stratmann, K. Bohnenkamp, and H.-J. Engell, *Corros. Sci.*, **23**, 969 (1983).
7. J. Dünnwald and A. Otto, *Corros. Sci.*, **29**, 1167 (1989).
8. M. Stratmann, K. Bohnenkamp, and H.-J. Engell, *Corros. Sci.*, **23**, 969 (1983).
9. M. Stratmann and K. Hoffmann, *Corros. Sci.*, **29**, 1329 (1989).
10. A. Kuch, *Corros. Sci.*, **28**, 221 (1988).
11. C. A. Melendres, M. Pankuch, Y. S. Li, and R. L. Knight, *Electrochim. Acta*, **37**, 2747 (1992).
12. D. L. A. de Faria, S. Venâncio Silva, and M. T. de Oliveira, *J. Raman Spectrosc.*, **28**, 873 (1997).
13. M. E. Vela, J. R. Vilche, and A. J. Arvia, *Electrochim. Acta*, **31**, 1633 (1986).
14. H. Antony, L. Legrand, L. Marchal, S. Perrin, P. Dillmann, and A. Chauss, *Electrochim. Acta*, **51**, 745 (2005).
15. M. Cohen and K. Hashimoto, *J. Electrochem. Soc.*, **121**, 42 (1974).
16. L. Martinez, D. Leinen, F. Martin, M. Gabas, J. Ramos-Barrado, E. Quagliata, and E. Dalchiele, *J. Electrochem. Soc.*, **154**, D126 (2007).
17. U. Schwertmann and R. M. Cornell, Iron oxides in the laboratory – Preparation and characterization, VCH Verlagsgesellschaft, Weinheim (1991).
18. M. K. Nieuwoudt, J. D. Comins, and I. Cukrowski, *J. Raman Spectrosc.*, **42**, 1335 (2011).
19. D. M. Sherman and T. D. Waite, *Am. Mineral.*, **70**, 1262 (1985).
20. M. A. Legodi and D. de Waal, *Dyes Pigm.*, **74**, 161 (2007).
21. M. Hanesch, *Geophys. J. Int.*, **177**, 941 (2009).
22. G. Nauer, P. Strecha, N. Brinda-Konopik, and G. Liptay, *J. Therm. Anal.*, **30**, 813 (1985).
23. M. Bouchard and D. C. Smith, *Spectrochim. Acta A*, **59**, 2247 (2003).
24. S. J. Oh, D. C. Cook, and H. E. Townsend, *Hyperfine Interact.*, **112**, 59 (1998).
25. A. P. Lee, J. Webb, D. J. Macey, W. van Bronswijk, A. R. Savarese, and G. C. de Witt, *J. Biol. Inorg. Chem.*, **3**, 614 (1998).
26. A. Periasamy, S. Muruganand, and M. Palaniswamy, *Rasayan J. Chem*, **2**, 981 (2009).
27. J. M. Dudik, C. R. Johnson, and S. A. Asher, *J. Chem. Phys.*, **82**, 1732 (1985).
28. N. Buzgar, A. Buzatu, and I. V. Sanislav, *An. Stiint. U. Al. I-Mat*, **55**, 5 (2009).
29. M. S. Odziemkowski, T. T. Schuhmacher, R. W. Gillham, and E. J. Reardon, *Corros. Sci.*, **40**, 371 (1998).
30. H. D. Lutz, H. Mller, and M. Schmidt, *J. Mol. Struct.*, **328**, 121 (1944).
31. L. J. Oblonsky and T. M. Devine, *Corros. Sci.*, **37**, 17 (1995).
32. P. Chen, K. Xu, X. Li, Y. Guo, D. Zhou, J. Zhao, X. Wu, C. Wu, and Y. Xie, *Chem. Sci.*, **5**, 2251 (2014).
33. E. R. Encina, M. Distaso, R. N. Klupp Taylor, and W. Peukert, *Cryst. Growth Des.*, **15**, 194 (2015).
34. J.-P. Jolivet, C. Chanéac, and E. Tronc, *Chem. Commun.*, (5), 481 (2004).